inorganics

MDPI

Article

Allosteric Fluorescent Detection of Saccharides and Biomolecules in Water from a Boronic Acid Functionalized Arene Ruthenium Assembly Hosting Fluorescent Dyes †

Alaa Maatouk, Thibaud Rossel and Bruno Therrien *

Institute of Chemistry, University of Neuchatel, Ave. de Bellevaux 51, CH-2000 Neuchatel, Switzerland; alaa.maatouk@unine.ch (A.M.); thibaud.rossel@unine.ch (T.R.)

* Correspondence: bruno.therrien@unine.ch

† This article is dedicated to Reinhard Neier on the occasion of his 75th birthday.

Abstract: A water-soluble arene ruthenium metalla-rectangle (MR1) functionalized with boronic acid groups was used to host various fluorescent dyes (fluorescein, eosin Y, and erythrosin B). These simple host–guest systems partially quench the natural fluorescence of the dyes, which can be regained in the presence of saccharides, phosphorylated molecules, and other analytes. The intensity of the regained fluorescence is directly linked to the nature of the analyte, and it shows some dose–response relationships with saccharides and phosphorylated molecules that are not compatible with a displacement assay, thus suggesting an allosteric mechanism. Interestingly, when fluorescein is trapped by the metalla-rectangle in the presence of D-fructose, half of the maximum fluorescence intensity is recovered at a fructose concentration of 17.2 ± 4.7 μM, while, for D-glucose, a concentration of 50.6 ± 2.5 μM is required for the same effect. Indeed, all combinations of analyte–host–dye (seven analytes, one host, three dyes) show a unique dose–response relationship in water at pH 8.0. However, in the presence of naphthalene and pyrene, fluorescein⊂MR1 shows a different behavior, acting as an indicator displacement assay with the full recovery of fluorescence. All data were analyzed by unsupervised machine learning technologies (PCA and cluster analysis), suggesting that such systems with multiple analyte–response behaviors are offering new perspectives for the development of highly sensitive, easily tunable, water-soluble, fluorescent-based sensing arrays for biomolecules and other analytes.

Keywords: saccharides; phosphorylated molecules; fluorescent dyes; coordination-driven self-assembly; allostery; displacement assay; sensing

Academic Editor: Alex Chun-Yuen Wong

Received: 4 December 2024
Revised: 17 December 2024
Accepted: 18 December 2024
Published: 24 December 2024

Citation: Maatouk, A.; Rossel, T.; Therrien, B. Allosteric Fluorescent Detection of Saccharides and Biomolecules in Water from a Boronic Acid Functionalized Arene Ruthenium Assembly Hosting Fluorescent Dyes. *Inorganics* **2025**, *13*, 1. https://doi.org/10.3390/inorganics13010001

1. Introduction

Nature provides the most advanced biological engineering technology, thanks to Darwinian evolution over millions of years [1]. Proteins are certainly one of the best engineered machineries created by nature, showing multiple functions and long-distance regulation mechanisms. The ability for proteins to change conformation and to trigger different responses to stimuli has been coined "allostery" [2,3]. Therefore, in an attempt to mimic nature, chemists have been trying to develop allosteric systems, in which an event on one part of the molecule generates a second event elsewhere [4,5], taking notable advantages on second coordination sphere interactions [6–8]. Such cascades of events are particularly attractive for sensing technology, where selectivity and sensitivity are crucial for discriminating between analytes [9–11]. However, to succeed, variable responses have to be produced by the sensor in the presence of analytes, to be able to generate a versatile

sensing array [12–15]. With the emergence of rational design coupled with high-throughput screening and combinatorial chemistry [16,17], we can now take advantage of artificial intelligence and robotics in chemistry to develop such sensing arrays [18]. In this context, we can now envisage the development of sensors based on allosteric mechanisms, thus expanding the chemical universe of sensors [19,20].

Coordination-driven self-assembly (CDSA) is particularly suitable for developing sensors [21–26]. Most CDSAs possess a cavity where a guest compound can sit, offering a primary binding site [27–29], while functionalization at the periphery of the CDSA can generate additional binding sites for either analytes or fluorescent probes [30–34]. Accordingly, the interaction of analytes or probes with CDSA will modify their conformational structure and physical property, thus potentially triggering chemical responses [35]. Moreover, the attractiveness of most CDSA synthetic strategies resides in their ability to interchange building blocks, thus facilitating a modulating approach with combinatorial aptitude [36,37]. This is particularly true with arene ruthenium assemblies, which are commonly built from three components [38], the arene ruthenium units, spacers (tetradentate bridging ligands), and linkers (bis-, tris-, tetra-pyridyl ligands), thus offering numerous possibilities to add functional groups and to modify the solubility, shape, and size of the assembly [39–41].

In sensing, several key challenges are still opened, like the specific detection of saccharides, dioxins, quinones, or phosphates, which are all highly difficult analytes to discriminate from topological competitors [42–44]. When dealing with saccharides, most sensors exploit the unique affinity of boronic acid for diols to generate boronate esters [45]. Since the first publication of a boronic acid-based sensor for saccharides in the 1990s [46], the number of publications in the field has grown tremendously. In parallel, the sophistication of the sensors has increased drastically, moving from one to two boronic acid functions per sugars to increase the binding affinity [47], to sensors with a nitrogen atom next to the boronic acid active site [48–50], to sensors incorporating fluorescent probes for rapid visual detection [51–54], to sensors exploiting indicator displacement assay mechanisms [55–57], to sensors with redox active functional groups [58–60], or to hybrid materials incorporating multiple boronic acid functions [61–65]. Therefore, to develop a new family of sensors, we have used a different scaffold: A water-soluble coordination-driven arene ruthenium assembly functionalized with boronic acids. Then, we have studied its ability to sense various analytes, from saccharides to phosphorylated molecules as well as planar aromatics.

2. Results

The synthesis of the boronic acid functionalized metalla-rectangle $[\{Ru(p\text{-cymene})\}_4(bpe)_2(babo)_2]^{4+}$ (MR1) is straightforward (Scheme 1). It is performed in methanol at reflux, by mixing the dinuclear complex $[\{Ru(p\text{-cymene})\}_2(babo)Cl_2]$ (babo-H_2 = *N*,*N*′-bis{4-(4,4,5,5-tetramethyl-1,3,2-dioxaborolan-2-yl)benzyl}oxalamide) with 1,2-bis(4-pyridyl)ethylene (bpe) in the presence of silver triflate (see the SI for full description and characterization). The tetracationic complex is isolated as its triflate salt in excellent yield (94%). The stereogenic nature of the ruthenium atoms reduces the symmetry, thus complicating the ^{1}H NMR spectrum (Figure S12). Nevertheless, the corresponding DOSY (diffusion-ordered spectroscopy) shows a single compound in solution (Figure S14), supporting the formation of MR1. Moreover, multiple peaks in the ESI-MS spectrum (Figure S16) confirm the formation of the assembly, especially the one at m/z = 720.15, which correspond to $[MR1 + CF_3SO_3]^{3+}$ (Figure S26a) and at m/z = 830.58 for the host–guest fluorescein⊂MR1 system $[MR1 + fluorescein + CF_3SO_3]^{3+}$ (Figure S26b). Such multiple-charged peaks of intact arene ruthenium metalla-assembly plus counter anions with or without guests are commonly observed with arene ruthenium assemblies [66,67].

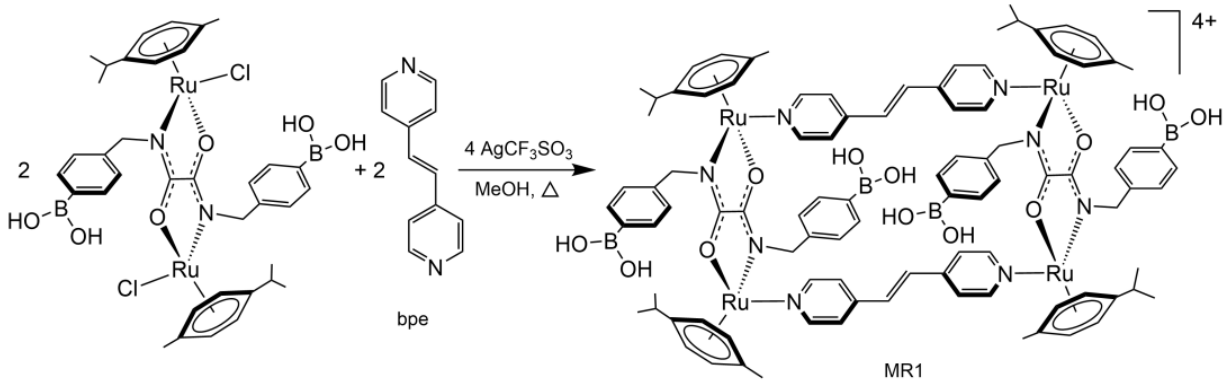

Scheme 1. Synthesis of metalla-rectangle MR1, see the SI for more details.

Then, three fluorescent dyes (fluorescein, eosin Y, and erythrosin B) were added to MR1 to form the corresponding host–guest systems, fluorophore⊂MR1. Interestingly, the quenching of the fluorescence for a 1:1 host–guest ratio was not total in water at pH 8.0 (HEPES buffer), and the encapsulation process of the dyes have shown different dynamic behaviors. In the case of fluorescein, heating at 35 °C overnight was required to reach equilibrium, and the fluorescence was quenched by 34% (Tables S1 and S2). On the other hand, for eosin Y and erythrosin B, an equilibrium was reached in only two hours at room temperature, with quenching values of 14% and 17%, respectively. The quenching behavior for a 1:1 MR1: fluorophore ratio has raised questions on the nature of the host–guest interactions and the location of the fluorophore in MR1. Therefore, further studies involving MR1 and fluorophores were conducted to better understand the interactions that take place in water (pH 8.0) between the fluorophore and MR1.

We have first evaluated the maximum quenching capacity of MR1 with fluorophores. A gradual addition of fluorescein to an aqueous solution containing MR1 showed that maximum quenching (≈ 50%) is reached when 2 equivalents of fluorescein are added (Figure S18). Similar results were obtained with eosin Y and erythrosin B, where maximum quenching was clearly obtained with two equivalents of fluorophore (Figure S18). Therefore, one can assume that each face of MR1, and accordingly up to two boronic acid functions, interacts with a fluorophore, thus forming overall (fluorophore)$_2$⊂MR1 aggregates under these conditions. In these aggregates, the boronic acid functions are probably acting as Lewis acid, thus forming at pH 8.0 new B$^-$-O bonds with the anionic fluorophore [68]. Indeed, to corroborate this assumption, we also looked at the quenching capacity of MR1 at pH 7.5 and 9.5, respectively. In both cases, no significant quenching effect was observed, thus suggesting that at pH 8.0 the boronic acid groups interact preferentially with the anionic form of the fluorophore instead of water (H_2O at pH 7.5 and OH^- at pH 9.5), a well-known phenomenon in boronic acid–saccharide chemistry [69]. Therefore, to keep one side of the assembly and boronic acid functions free for interacting with analytes, we have focused our attention to 1:1 fluorophore⊂MR1 systems (Figure 1), working in aqueous solution at pH 8.0 in the presence of HEPES buffer.

We have screened the three fluorophores⊂MR1 systems with multiple analytes (D-fructose, D-glucose, D-galactose, D-ribose, sodium triphosphate, D-ribose-5-phosphate, adenosine triphosphate) and determined the binding affinity by fluorescence spectroscopy (Figure 2). The fluorophore⊂MR1 sensors were dissolved in HEPES (10 mM solution, pH = 8.0) to a final concentration of 25 μM, and 1 to 10 equivalents of analytes were incrementally added to the mixture (see SI for more details). The initial fluorescence of the fluorophore⊂MR1 sensor was systematically subtracted, and only the regained fluorescence was used to plot the sensing ability of fluorophore⊂MR1 and to determine the effective concentration (EC_{50}) of the sensors (Table 1).

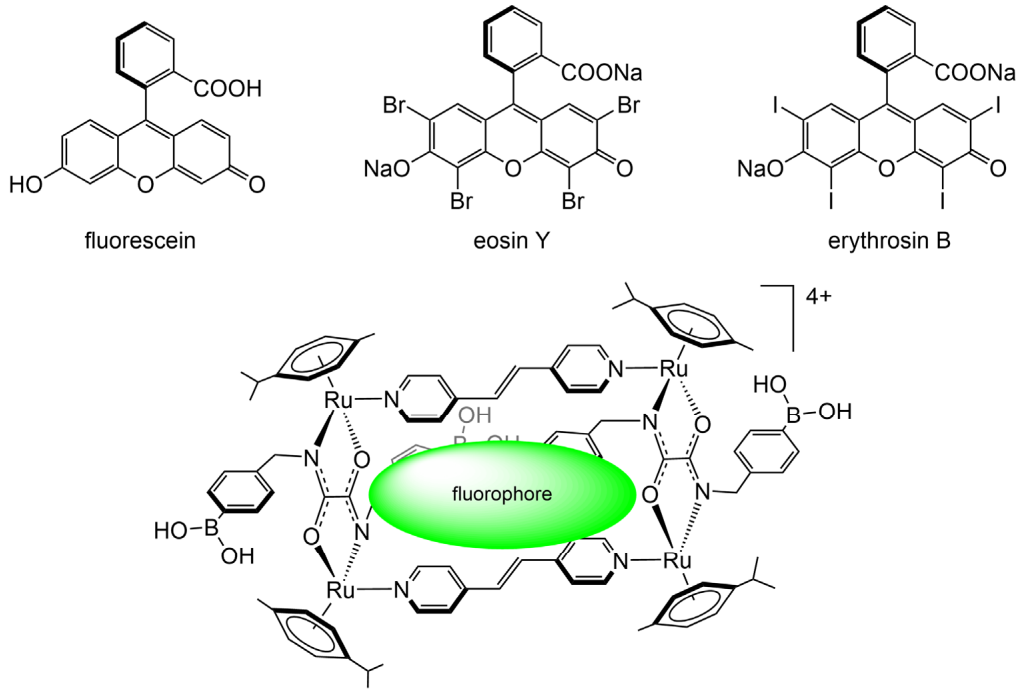

Figure 1. Fluorescent dyes and schematic representation of the 1:1 fluorophore⊂MR1 systems.

Table 1. EC_{50} values (triplicates) and the corresponding heat map chart of the fluorophore⊂MR1 systems titrated with analytes.

		A	B	C
	analyte	fluorescein⊂MR1	eosin Y⊂MR1	erythrosin⊂MR1
1	D-fructose	17.2 ± 4.7 µM	50.9 ± 4.4 µM	79.7 ± 6.7 µM
2	D-glucose	50.6 ± 2.5 µM	n.d.	30.6 ± 1.4 µM
3	D-galactose	37.0 ± 4.1 µM	n.d.	61.4 ± 9.2 µM
4	D-ribose	24.3 ± 2.0 µM	63.8 ± 4.8 µM	64.6 ± 4.3 µM
5	sodium triphosphate	48.9 ± 3.8 µM	61.4 ± 9.3 µM	40.6 ± 2.2 µM
6	D-ribose-5-phosphate	24.3 ± 2.0 µM	110.5 ± 7.8 µM	50.1 ± 5.1 µM
7	adenosine triphosphate	53.9 ± 11.3 µM	62.1 ± 3.7 µM	66.4 ± 4.7 µM

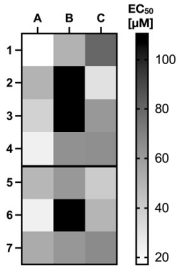

As presented in Figure 2, all fluorophore⊂MR1 sensors show a different dose–response curve for each analyte, as well as substantial differences in efficacy. This is better illustrated when looking at the EC_{50} values and the corresponding heat map chart (Table 1). The weakest response was observed between D-ribose-5-phosphate and eosin Y⊂MR1 (110.5 ± 7.8 µM), followed by D-fructose with the erythrosin B⊂MR1 system (79.7 ± 6.7 µM). On the other hand, the lowest EC_{50} values, which correspond to higher efficacy, were observed for D-fructose with fluorescein⊂MR1 (17.2 ± 4.7 µM) and D-glucose with erythrosin B⊂MR1 (30.6 ± 1.4 µM). In the case of D-glucose and D-galactose with eosin Y⊂MR1, no clear inflexion points were observed (Figure 2b), and accordingly, no EC_{50} values determined. This behavior suggests that the interaction between eosin Y and MR1 is negligibly affected by the presence of these two analytes. Such behavioral differences between sensors and analytes are clearly the premises for developing fluorescent-based sensing arrays.

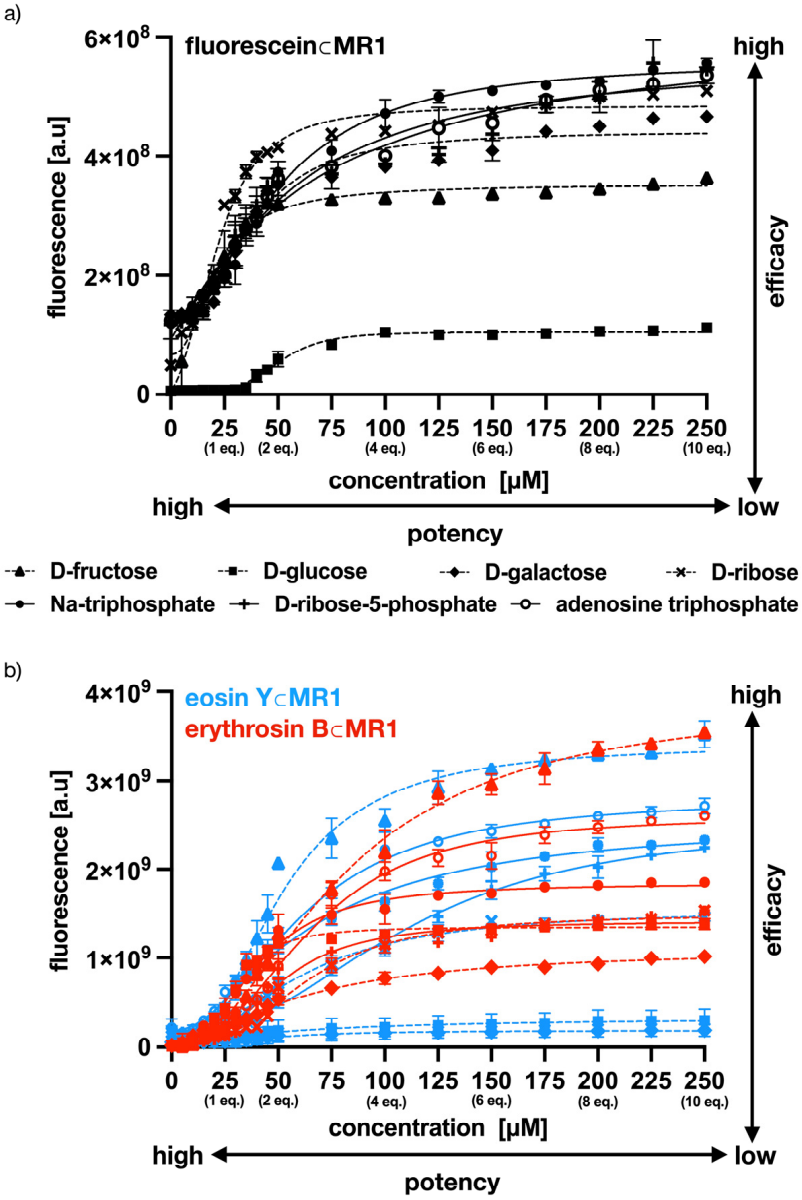

Figure 2. Titrations of various analytes in the presence of (**a**) fluorescein⊂MR1 (25 μM conc., λ_{ex} = 498 nm, λ_{em} = 515 nm), (**b**) eosin Y⊂MR1 (25 μM conc., λ_{ex} = 498 nm, λ_{em} = 515 nm) and erythrosin B⊂MR1 (25 μM conc., λ_{ex} = 498 nm, λ_{em} = 554 nm), in triplicate at pH = 8.0 (HEPES buffer).

Moreover, from Figure 2a, we can observe a clear discrepancy between the shape of the dose–response curves; the saccharides (dotted lines) are rapidly flattening after the addition of a second equivalent of analyte (50 μM), while for the phosphorylated molecules, 10 equivalents of analytes (solid lines) are just enough to reach a plateau. This can be linked to the binding mode of these analytes with the fluorescein⊂MR1 system. For sugars, it is well-known that boronic acids form up to two bonds with diols to generate stable boronate esters [70], while with phosphates, a single bond is formed with higher lability [71–74]. Therefore, as suggested by the shape of these dose–response curves, different analytes prompt different responses from the fluorescein⊂MR1 sensor, most likely by conformational changes. The sugars seem to interact strongly with the free boronic acid functions of MR1, thus having a variable impact on the partial quenching of the fluorescence, which remains stable after two equivalents of analytes. In the case of phosphorylated molecules, interactions appear to be weaker, as more equivalents of analytes are needed to reach an equilibrium, but they also show a higher impact on the

quenching process. Therefore, we can conclude that different dynamic processes are taking place, depending on the nature of the analyte (see Figure 7).

To confirm the importance of the boronic acid functions, a known cationic metalla-rectangle with four hydroxy ethyl groups was prepared [67] and tested with fluorescein as fluorophore, in the presence or absence of the same analytes (Figure 3). This metalla-rectangle (MR2), which possesses a cavity similar to that of MR1, interacts with fluorescein, showing partial quenching of the fluorescence (≈12%). However, maximum quenching was reached after the addition of only one equivalent of the fluorophore (Figure S19), suggesting that fluorescein sits in the cavity of MR2 and interacts mainly by π-stacking and electrostatic interactions, and not with the hydroxyl groups at the periphery of the rectangle. Accordingly, upon the gradual addition of analytes, the quenching of fluorescence remains the same, having no effect on the host–guest interactions and the photophysical property of the fluorescein⊂MR2 system (Figure 3). Overall, these results confirm that another mode of interaction between the fluorophore and the non-boronic acid functionalized metalla-rectangle MR2 is in action here, as compared to the fluorescein⊂MR1 system (see Figure 7). These results support our design, in which boronic acid functional groups are crucial for sensing saccharides and to some extent phosphorylated molecules, and that such analytes can disrupt the quenching property of the fluorophore⊂MR1 systems by allosteric mechanisms.

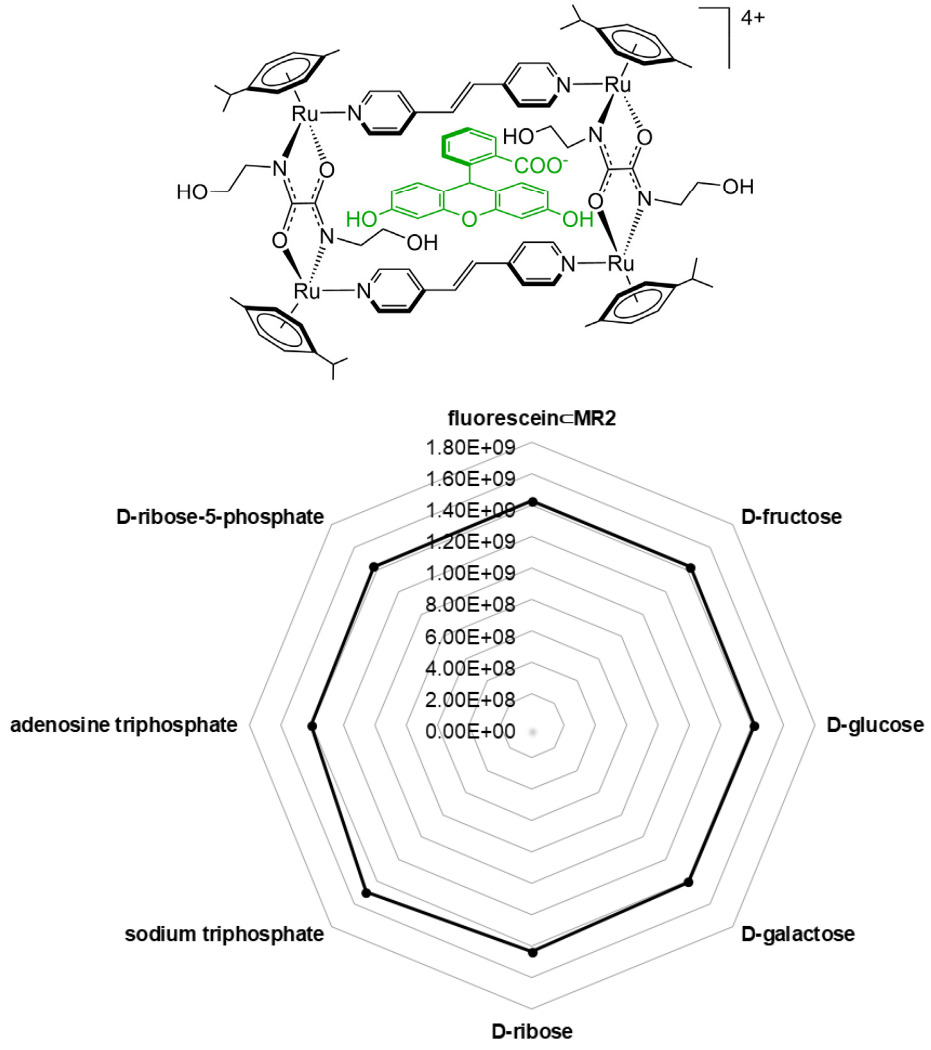

Figure 3. Structure of fluorescein⊂MR2 (top) and its response (25 μM conc., λ_{ex} = 498 nm, λ_{em} = 515 nm) to analytes (>10 eq.) at pH 8.0 (HEPES buffer), at room temperature.

Then, we have focused our attention to other analytes, especially those who are not expected to interact with boronic acid functions, such as planar aromatic molecules. In the past, pyrene and naphthalene have shown strong interactions with the hydrophobic cavity of arene ruthenium assemblies, showing excellent binding affinity [75]. Titrations of fluorescein⊂MR1 with naphthalene and pyrene (Figure 4) show another dose–response than those observed for saccharides and phosphorylated molecules, consistent with displacement assays (see Figure 7), despite the poor solubility of planar aromatics in aqueous solutions (1% DMF). A DOSY experiment supports the displacement mechanism, which, upon the addition of five equivalents of naphthalene to a CD_3OD solution of fluorescein⊂MR1, a new diffusion coefficient is observed, where fluorescein is no more attached to MR1 and is replaced by naphthalene (Figures S24 and S25). This result suggests that, upon encapsulation of pyrene or naphthalene in the hydrophobic cavity of MR1, the binding of fluorescein to the boronic acid functionalized MR1 assembly is weakened, and fluorescein is eventually released from the fluorescein⊂MR1 adduct. In addition, it shows that the solvent is another variable that can be used to modulate the sensing mechanisms.

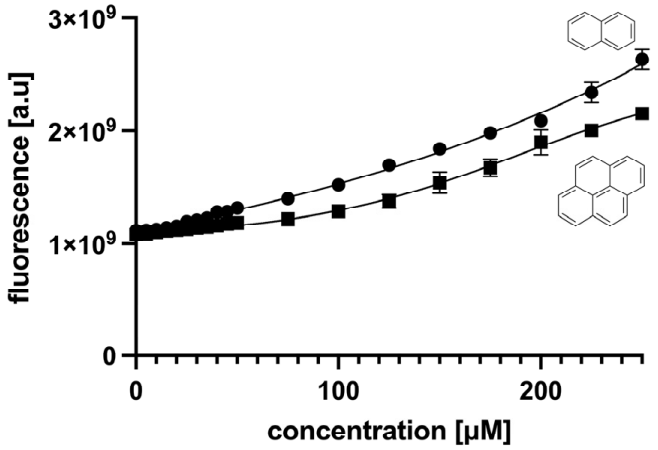

Figure 4. Titrations of naphthalene and pyrene with fluorescein⊂MR1 at room temperature in HEPES buffer at pH 8.0 (1% DMF, 25 µM conc., λ_{ex} = 498 nm, λ_{em} = 515 nm).

Considering the facility to combine arene ruthenium metalla-rectangles (MR1, MR2) with fluorophores (fluorescein, eosin Y, erythrosin B) and the rapidity to measure the variation of fluorescence to evaluate the sensing ability of the host–guest systems with multiple analytes (D-fructose, D-glucose, D-galactose, D-ribose, sodium triphosphate, D-ribose-5-phosphate, adenosine triphosphate, naphthalene, pyrene), a considerable amount of data was acquired in a reasonable timeframe. Therefore, we have used online unsupervised machine learning technology to analyze and reduce the dimensionality of the data and to draw some conclusions [76]. In this context, three categories of data were identified from the main titration experiments: EC_{50}, Hill slope, and fluorescence variation (ΔF_{max}). The analysis revealed that the three principal components accounted for over 85% of the total variance, indicating a significant reduction in complexity, while retaining most of the information. Specifically, the first component was heavily influenced by the EC_{50} values, suggesting that this metric possesses the main variability. The second and third principal components were predominantly associated with the Hill slope and ΔF_{max}, respectively (Figure 5). The insights gained from PCA analysis highlighted the critical role of EC_{50} in differentiating analytes, with Hill slope and ΔF_{max} providing additional nuances, being fully consistent with the visual analysis of the dose–response titrations (Figure 2, Table 1).

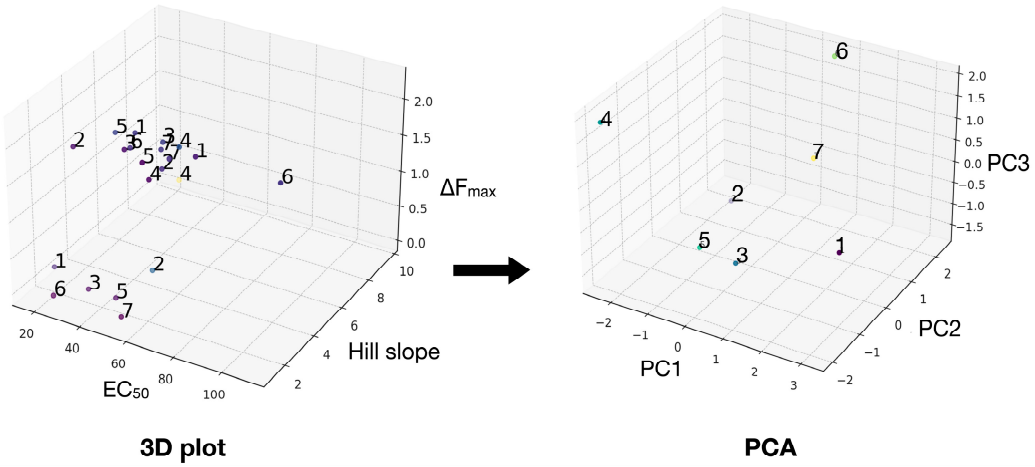

Figure 5. PCA analysis of the data with chatGPT-4o [76].

In addition, to better understand the structure and relationships within our dataset, we performed a clustering analysis using K-means clustering [77]. This method allows us to group similar data points, providing insights into the underlying patterns and potential subgroups within the data. The K-means algorithm was applied to the transformed data with three clusters, the number of clusters based on the elbow method [78]. The clustering was performed on the standardized values of the principal components, showing three distinct groups within the dataset. This clustering analysis is visualized using a 3D scatter plot (Figure 6). The following key observations are made for each cluster. Cluster 0 includes analytes that exhibit high EC_{50} values (low efficacy) and a variable range of ΔF_{max} values. In cluster 1, the analytes show moderate EC_{50} values and average Hill slopes, while ΔF_{max} are high. Finally, analytes in cluster 2 have low EC_{50}, low Hill slopes, and variable ΔF_{max}. These clusters represent groups of analytes with similar recognition profiles, characterized by their EC_{50}, Hill slope, and ΔF_{max} values. The visualization of these clusters provides valuable insights into the diversity and similarity among the analytes, helping to identify potential candidates for further investigations. Furthermore, this analysis highlights the importance of combining dimensionality reduction techniques, like PCA, with clustering algorithms to uncover meaningful patterns in complex datasets [79,80].

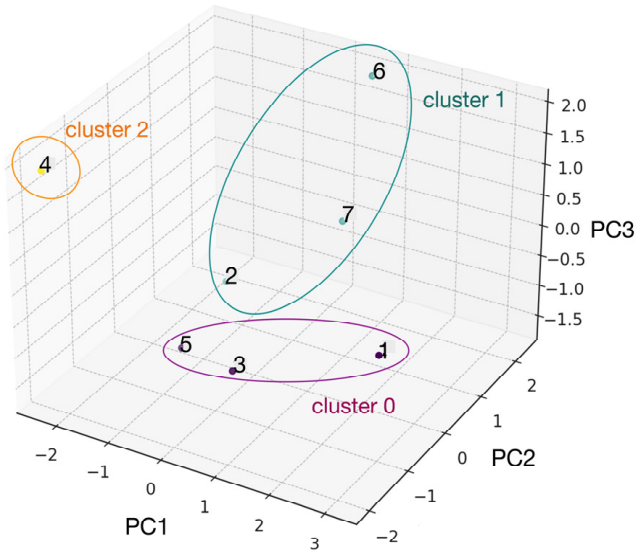

Figure 6. K-means clustering from the PCA.

3. Materials and Methods

Commercially available solvents were purchased from Sigma-Aldrich® (St. Louis, MO, USA) and Fisher Scientific® (Waltham, MA, USA). All reagents and chemicals were purchased from Sigma Aldrich or Chemie Brunschwig AG® (Basel, Switzerland), while the fluorescent dyes (fluorescein, eosin Y, erythrosin B) were purchased from Acros Organics® (Geel, Belgium). All chemicals were used as received. Normal phase column chromatography was performed on a combiflash system with sfär 25 g cartridges purchased from Biotage® in Uppsala (Sweden). The (*p*-cymene)ruthenium chloride dimer [67], and the tetracationic metalla-rectangle MR2 [81], were prepared according to published methods (see the SI for full description and characterization of the compounds).

The ^{1}H, $^{13}C\{^{1}H\}$ and DOSY NMR spectra were recorded on a Bruker Avance II 600 MHz at 20 °C in $CDCl_3$ (7.2 ppm), CD_3OD (3.3 ppm), DMSO-d_6 (2.5 ppm), or $(CD_3)_2CO$ (2.0 ppm) relative to residual solvents. The $^{11}B\{^{1}H\}$ NMR spectra were recorded on a Bruker Avance II 400 MHz spectrometers at 20 °C at the department of Chemistry, Biochemistry and Pharmacy in Bern (Switzerland). Multiplicities are reported in Hz as: s = singlet, d = doublet, t = triplet, q = quartet and m = multiplet. Electrospray ionization mass spectra were obtained in positive ion mode on an LTQ Orbitrap Elite instrument at the ISIC Mass Spectrometry Service (SSMI) in Lausanne (Switzerland).

Fluorescence measurements were carried out in black NUNC® 96 well plates using VICTOR® Nivo™ multimode plate reader. The instrument was stabilized to the required temperature (20 °C or 35 °C) for each measurement. All measurements were done at least in triplicate. Fluorescence spectra were recorded using an excitation wavelength of λ_{ex} = 498 nm for fluorescein and λ_{ex} = 525 nm for erythrosin B and eosin Y. The intensity of the fluorophore emission peak at λ_{em} = 515 nm for fluorescein and λ_{em} = 554 nm for erythrosine B and eosin Y was used to determine the binding constants for all analytes. Determination of binding constants for each analyte (displacement assay, dose-response assay) was carried out using Prism 5.0® version 10.2.1 for Mac (GraphPad Software).

Stock solutions of rectangles (0.1 M) were prepared in organic solvents, DMF for MR1 and CH_3CN for MR2. Stock solutions of analytes and fluorophores were prepared in distilled water (0.1 M). Working solutions of rectangles, fluorophores and analytes were obtained by dilution of the 0.1 M stock solutions using 10 mM HEPES buffers at different pHs. The pH of the HEPES solutions was adjusted using solid NaOH and controlled with a FiveEasy METTLER TOLEDO® pH meter (see the SI for further details).

The association constants (K_a) were determined in black NUNC® 96 well plates and the fluorescence was monitored with a thermostatted VICTOR® Nivo™ multimode plate reader. The maximal fluorescence of the fluorophore⊂MR was measured after 2 h of reaction with λ_{ex} = 498 nm and λ_{em} = 515 nm for fluorescein, λ_{ex} = 525 nm and λ_{em} = 554 nm for erythrosin B and eosin Y. Determination of K_a were performed using a one-to-one binding model [81] (all graphics, titrations, and other experiments are described and presented in the SI).

4. Conclusions

Hybrid sensors, combining an arene ruthenium CDSA functionalized with boronic acid groups and fluorophore guests, have been synthesized and characterized. The fluorophore⊂MR1 adducts show interesting responses to analytes, acting like indicator displacement assays with planar aromatic molecules, while, with saccharides, an allosteric mechanism is taking place (Figure 7). With saccharides, the free boronic acids interact with diols forming two B-O bonds, only disrupting the fluorophore–MR1 photophysical property without forcing dissociation of the fluorophore⊂MR1 adduct. On the other hand, with planar aromatic molecules, different interactions are involved, which free the fluorophore

when sufficient amounts of analyte are added, thus acting as an indicator displacement assay. In the case of phosphorylated molecules, the system behaves differently, showing mixed responses.

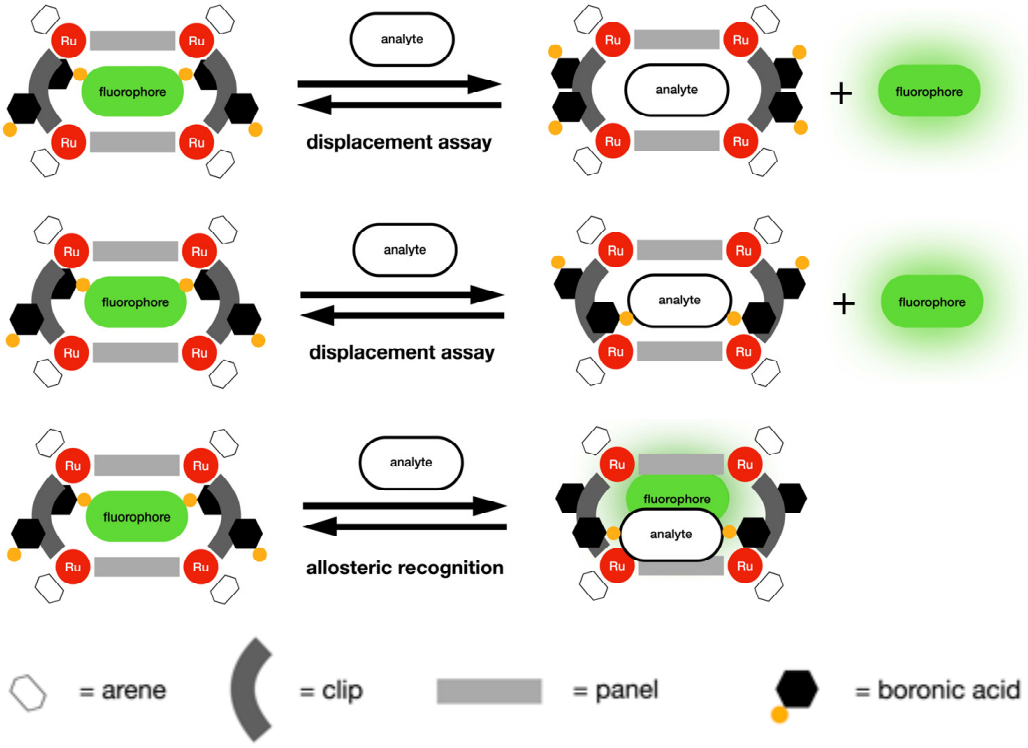

Figure 7. Schematic representation of the proposed mechanisms involved in the fluorophore⊂MR1 system (top, standard displacement assay; middle, hybrid displacement assay with boronic acid interactions; bottom, allosteric mechanism).

Supplementary Materials: The following supporting information can be downloaded at: https://www.mdpi.com/article/10.3390/inorganics13010001/s1, Synthesis and characterization of all compounds, NMR data (^{1}H, ^{13}C{^{1}H}, ^{11}B{^{1}H}, DOSY), ESI spectra, titrations, and association and dissociation constants.

Author Contributions: Conceptualization, B.T. and T.R.; methodology, A.M. and T.R.; validation, A.M., T.R. and B.T.; formal analysis, A.M. and T.R.; data curation, A.M. and T.R.; writing—original draft preparation, A.M., T.R. and B.T.; writing—review and editing, B.T.; visualization, A.M., T.R. and B.T.; supervision, T.R. and B.T.; project administration, B.T. All authors have read and agreed to the published version of the manuscript.

Funding: This research received no external funding.

Data Availability Statement: The data supporting this article have been included as part of the Supplementary Materials [81,82].

Acknowledgments: We thank the University of Neuchatel for financial support.

Conflicts of Interest: The authors declare no conflicts of interest.

References

1. A Castle, S.D.; Stock, M.; Gorochowski, T.E. Engineering is evolution: A perspective on design processes to engineer biology. *Nat. Commun.* **2024**, *15*, 3640. [CrossRef] [PubMed]
2. Monod, J.; Wyman, J.; Changeux, J.-P. On the nature of allosteric transitions: A plausible model. *J. Mol. Biol.* **1965**, *12*, 88–118. [CrossRef] [PubMed]

3. Ebrahim, S.; Samanta, D. Engineering protein-based therapeutics through structural and chemical design. *Nat. Commun.* **2023**, *14*, 2411. [CrossRef]
4. Fisher, G.; Corbella, M.; Alphey, M.S. Allosteric rescue of catalytically impaired ATP phosphoribosyltransferase variants links protein dynamics to active-site electrostatic preorganisation. *Nat. Commun.* **2022**, *13*, 7607. [CrossRef]
5. Ke, C.; Destecroix, H.; Crump, M.; Davis, A.P. A simple and accessible synthetic lectin for glucose recognition and sensing. *Nat. Chem.* **2012**, *4*, 718–723. [CrossRef]
6. Kremer, C.; Lützen, A. Artificial Allosteric Receptors. *Chem. Eur. J.* **2013**, *19*, 6162–6196. [CrossRef]
7. Tsai, C.-J.; Del Sol, A.; Nussinov, R. Protein allostery, signal transmission and dynamics: A classification scheme of allosteric mechanisms. *Mol. BioSyst.* **2009**, *5*, 207–216. [CrossRef]
8. Kimura, Y.; Matsumura, K.; Ono, K.; Tsuchido, Y.; Ka-wai, H. Recognition of Amino Acid Salts by Temperature-Dependent Allosteric Binding with Stereodynamic Urea Receptors. *Chem. Eur. J.* **2024**, *30*, e202400154. [CrossRef]
9. Musikavanhu, B.; Liang, Y.; Xue, Z.; Feng, L.; Zhao, L. Strategies for Improving Selectivity and Sensitivity of Schiff Base Fluorescent Chemosensors for Toxic and Heavy Metals. *Molecules* **2023**, *28*, 6960. [CrossRef]
10. Thangadurai, T.D.; Manjubaashini, N. Progressions in chemical and biological analytes sensing technology based on nanostructured materials: A comprehensive review. *Mater. Sci. Eng.* **2021**, *271*, 115307. [CrossRef]
11. Sun, X.; James, T.D. Glucose Sensing in Supramolecular Chemistry. *Chem. Rev.* **2015**, *115*, 8001–8037. [CrossRef] [PubMed]
12. Yu, L.; Wang, S.; Huang, K.; Liu, Z.; Gao, F.; Zeng, W. Fluorescent probes for dual and multi analyte detection. *Tetrahedron* **2015**, *71*, 4679–4706. [CrossRef]
13. Krämer, J.; Kang, R.; Grimm, L.M.; Cola, L.D.; Picchetti, P.; Biedermann, F. Molecular Probes, Chemosensors, and Nanosensors for Optical Detection of Biorelevant Molecules and Ions in Aqueous Media and Biofluids. *Chem. Rev.* **2022**, *122*, 3459–3636. [CrossRef] [PubMed]
14. Wu, X.; Li, Z.; Chen, X.-X.; Fossey, J.S.; James, T.D.; Jiang, Y.-B. Selective sensing of saccharides using simple boronic acids and their aggregates. *Chem. Soc. Rev.* **2013**, *42*, 8032. [CrossRef]
15. Fang, G.; Wang, H.; Bian, Z.; Sun, J.; Liu, H.; Fang, H.; Liu, B.; Yao, Q.; Wu, Z. Recent development of boronic acid-based fluorescent sensors. *RSC Adv.* **2018**, *8*, 29400–29427. [CrossRef]
16. Gordon, E.M.; Barrett, R.W.; Dower, W.J.; Fodor, S.P.A.; Gallop, M.A. Applications of Combinatorial Technologies to Drug Discovery. 2. Combinatorial Organic Synthesis, Library Screening Strategies, and Future Directions. *J. Med. Chem.* **1994**, *37*, 1385–1401. [CrossRef]
17. Potyrailo, R.; Rajan, K.; Stoewe, K.; Takeuchi, I.; Chisholm, B.; Lam, H. Combinatorial and High-Throughput Screening of Materials Libraries: Review of State of the Art. *ACS Comb. Sci.* **2011**, *13*, 579–633. [CrossRef]
18. Jin, X.; Liu, C.; Xu, T.; Su, L.; Zhang, X. Artificial intelligence biosensors: Challenges and prospects. *Biosens. Bioelectron.* **2020**, *165*, 112412. [CrossRef]
19. Lu, S.; Shen, Q.; Zhang, J. Allosteric Methods and Their Applications: Facilitating the Discovery of Allosteric Drugs and the Investigation of Allosteric Mechanisms. *Acc. Chem. Res.* **2019**, *52*, 492–500. [CrossRef]
20. Takeuchi, M.; Ikeda, M.; Sugasaki, A.; Shinkai, S. Molecular Design of Artificial Molecular and Ion Recognition Systems with Allosteric Guest Responses. *Acc. Chem. Res.* **2001**, *34*, 865–873. [CrossRef]
21. Sepehrpour, H.; Fu, W.; Sun, Y.; Stang, P.J. Biomedically Relevant Self-Assembled Metallacycles and Metallacages. *J. Am. Chem. Soc.* **2019**, *141*, 14005–14020. [CrossRef] [PubMed]
22. Mishra, A.; Lee, S.; Kim, H.; Cook, T.R.; Stang, P.J.; Chi, K.-W. Self-assembled metalla-bowls for selective sensing of multi-carboxylate anions. *Dalton Trans.* **2012**, *41*, 1195–1201. [CrossRef] [PubMed]
23. Paul, A.; Roy, S. Chirality Sensing in Coordination-driven Supramolecular Assemblies. *ChemRxiv* **2024**, *28*, 26434. [CrossRef]
24. Chang, X.; Zhou, Z.; Shang, C.; Wang, G.; Wang, Z.; Qi, Y.; Li, Z.-Y.; Wang, H.; Cao, L.; Li, X.; et al. Coordination-Driven Self-Assembled Metallacycles Incorporating Pyrene: Fluorescence Mutability, Tunability, and Aromatic Amine Sensing. *J. Am. Chem. Soc.* **2019**, *141*, 1757–1765. [CrossRef]
25. Shanmugaraju, S.; Bar, A.K.; Chi, K.-Y.; Mukherjee, P. Coordination-Driven Self-Assembly of Metallamacrocycles via a New Pt^{II}_2 Organometallic Building Block with 90° Geometry and Optical Sensing of Anions. *Organometallics* **2010**, *29*, 2971–2980. [CrossRef]
26. Imai, Y.; Nakano, Y.; Kawai, T.; Yuasa, J. A Smart Sensing Method for Object Identification Using Circularly Polarized Luminescence from Coordination-Driven Self-Assembly. *Angew. Chem. Int. Ed.* **2018**, *130*, 9111–9116. [CrossRef]
27. Inokuma, Y.; Kawano, M.; Fujita, M. Crystalline molecular flasks. *Nat. Chem.* **2011**, *3*, 349–358. [CrossRef]
28. Benchimol, E.; Tessarolo, J.; Zhang, B.; Clever, G.H. Photoswitchable coordination cages. *Nat. Chem.* **2024**, *146*, 6905–6911. [CrossRef]
29. Ludden, M.D.; Taylor, C.G.D.; Ward, M.D. Orthogonal binding and displacement of different guest types using a coordination cage host with cavity-based and surface-based binding sites. *Chem. Sci.* **2021**, *12*, 12640–12650. [CrossRef]

30. Luddena, M.D.; Ward, M.D. Outside the box: Quantifying interactions of anions with the exterior surface of a cationic coordination cage. *Dalton Trans.* **2021**, *50*, 2782–2791. [CrossRef]
31. Lee, S.G.; Lin, W. A Chiral Molecular Square with Metallo-Corners for Enantioselective Sensing. *J. Am. Chem. Soc.* **2002**, *124*, 4554–4555. [CrossRef] [PubMed]
32. Chen, L.-J.; Yang, H.-B. Construction of Stimuli-Responsive Functional Materials via Hierarchical Self-Assembly Involving Coordination Interactions. *Acc. Chem. Res.* **2018**, *51*, 2699–2710. [CrossRef] [PubMed]
33. Hu, Y.-X.; Zhang, X.; Xu, L.; Yang, H.-B. Coordination-Driven Self-Assembly of Functionalized Supramolecular Metallacycles: Highlighted Research during 2010–2018. *Isr. J. Chem.* **2018**, *59*, 209–219. [CrossRef]
34. Gao, Z.; Jia, J.; Fan, W.; Liao, T.; Zhang, Z. Zirconium metal organic cages: From phosphate selective sensing to derivate forming. *Chin. Chem. Lett.* **2022**, *33*, 4415–4420. [CrossRef]
35. Custelcean, R.; Bonnesen, P.V.; Duncan, N.C.; Zhang, X.; Watson, L.A.; Berkel, G.B.; Parson, W.B.; Hay, B.J. Urea-Functionalized M_4L_6 Cage Receptors: Anion-Templated Self-Assembly and Selective Guest Exchange in Aqueous Solutions. *J. Am. Chem. Soc.* **2012**, *134*, 8525–8534. [CrossRef]
36. Northrop, B.H.; Zheng, Y.-R.; Chi, K.-W.; Stang, P.J. Self-Organization in Coordination-Driven Self-Assembly. *Acc. Chem. Res.* **2009**, *42*, 1554–1563. [CrossRef]
37. Cook, T.R.; Stang, P.J. Recent Developments in the Preparation and Chemistry of Metallacycles and Metallacages via Coordination. *Chem. Rev.* **2015**, *115*, 7001–7045. [CrossRef]
38. Therrien, B. Unmasking Arene Ruthenium Building Blocks. *Chem. Rec.* **2021**, *21*, 460. [CrossRef]
39. Alvariño, C.; Heinrich, B.; Donnio, B.; Deschenaux, R.; Therrien, B. Supramolecular Arene-Ruthenium Metallacycle with Thermotropic Liquid-Crystalline Properties. *Inorg. Chem.* **2019**, *58*, 9505–9512. [CrossRef]
40. Xu, Y.; Li, C.; Lu, S.; Wang, Z.; Liu, S.; Yu, X.; Li, X.; Sun, Y. Construction of emissive ruthenium(II) metallacycle over 1000 nm wavelength for in vivo biomedical applications. *Nat. Commun.* **2022**, *13*, 2009. [CrossRef]
41. Yin, C.; Du, J.; Olenyuk, B.; Stang, P.J.; Sun, Y. The Applications of Metallacycles and Metallacages. *Inorganics* **2023**, *11*, 54. [CrossRef]
42. van Enter, B.J.; von Hauff, E. Challenges and perspectives in continuous glucose monitoring. *Chem. Commun.* **2018**, *54*, 5032–5045. [CrossRef] [PubMed]
43. Sakamoto, T.; Ojida, A.; Hamachi, I. Molecular recognition, fluorescence sensing, and biological assay of phosphate anion derivatives using artificial Zn(II)-Dpa complexes. *Chem. Commun.* **2009**, 141–152. [CrossRef] [PubMed]
44. Patrizi, B.; Siciliani de Cumis, M.; Viciani, S.; D'Amato, F. Dioxin and Related Compound Detection: Perspectives for Optical Monitoring. *Int. J. Mol. Sci.* **2019**, *20*, 2671. [CrossRef]
45. Brooks, W.L.A.; Deng, C.C.; Sumerlin, B.S. Structure-Reactivity Relationships in Boronic Acid-Diol Complexation. *ACS Omega* **2018**, *3*, 17863–17870. [CrossRef]
46. James, T.D.; Sandanayake, K.R.A.S.; Shinkai, S. Saccharide Sensing with Molecular Receptors Based on Boronic Acid. *Angew. Chem. Int. Ed.* **1996**, *35*, 1910–1922. [CrossRef]
47. Bian, Z.; Liu, A.; Li, Y.; Fang, G.; Yao, Q.; Zhang, G.; Wu, Z. Boronic acid sensors with double recognition sites: A review. *Analyst* **2020**, *145*, 719–744. [CrossRef]
48. Sun, X.; Chapin, B.P.; Metola, P.; Collins, B.; Wang, B.; James, T.D.; Anslyn, E.V. The mechanisms of boronate ester formation and fluorescent turn-on in ortho-aminomethylphenylboronic acids. *Nat. Chem.* **2019**, *11*, 768–778. [CrossRef]
49. James, T.D.; Sandnayake, K.R.A.S.; Iguchi, R.; Shinkai, S. Novel Saccharide-Photoinduced Electron Transfer Sensors Based on the Interaction of Boronic Acid and Amine. *J. Am. Chem. Soc.* **1995**, *117*, 8982–8987. [CrossRef]
50. Franzen, S.; Ni, W.; Wang, B. Study of the Mechanism of Electron-Transfer Quenching by Boron−Nitrogen Adducts in Fluorescent Sensors. *J. Phys. Chem. B* **2003**, *107*, 12942–12948. [CrossRef]
51. Bruen, D.; Delaney, C.; Diamond, D.; Florea, L. Fluorescent Probes for Sugar Detection. *ACS Appl. Mater. Interfaces* **2018**, *10*, 38431–38437. [CrossRef] [PubMed]
52. Xu, S.; Sedgwick, A.C.; Elfeky, S.A.; Fossey, J.S.; James, T.D. A boronic acid-based fluorescent hydrogel for monosaccharide detection. *Front. Chem. Sci. Eng.* **2020**, *14*, 112–116. [CrossRef]
53. Ouyang, F.; Zhang, X.; Wang, T.; Shuai, Q. A fluorescent turn on/off probe for glucose detection based on a boronic acid-capped 1,1′-ferrocenedicarboxylic acid functional graphene oxide. *Mater. Today Commun.* **2022**, *33*, 104681. [CrossRef]
54. Kashiwazaki, G.; Watanabe, R.; Nishikawa, A.; Kawamura, K.; Kitayama, T.; Hibi, T. A selective hybrid fluorescent sensor for fructose detection based on a phenylboronic acid and BODIPY-based hydrophobicity probe. *RSC Adv.* **2022**, *12*, 15083–15090. [CrossRef]
55. Rather, I.; Ali, R. Indicator displacement assays: From concept to recent developments. *Org. Biomol. Chem.* **2021**, *19*, 5926. [CrossRef]

56. Wikeley, S.M.; Przybylowski, J.; Lozano-Sanchez, P.; Caffio, M.; James, T.D.; Bull, S.D.; Fletcher, P.J.; Marken, F. Polymer indicator displacement assay: Electrochemical glucose monitoring based on boronic acid receptors and graphene form competitively binding with poly-nordihydroguaiaretic acid. *Analyst* **2022**, *147*, 661–670. [CrossRef]
57. Sedgwick, A.C.; Brewster, J.T., II; Wu, T.; Feng, X.; Bull, S.D.; Qian, X.; Sessler, J.L.; James, T.D.; Anslyn, E.V.; Sun, X. Indicator displacement assays (IDAs): The past, present and future. *Chem. Soc. Rev.* **2021**, *50*, 9–38. [CrossRef]
58. Egawa, Y.; Seki, T.; Takahashi, S.; Anzai, J. Electrochemical and optical sugar sensors based on phenylboronic acid and its derivatives. *Mater. Sci. Eng. C* **2011**, *31*, 1257–1264. [CrossRef]
59. Han, J.H.; Kim, C.H.; Min, C.H.; Kim, M.J.; Kim, S.; Ji, H.B.; Yoon, S.B.; Lee, C.; Choy, Y.B. Microneedles coated with composites of phenylboronic acid-containing polymer and carbon nanotubes for glucose measurements in interstitial fluids. *Biosens. Bioelectron.* **2023**, *238*, 115571. [CrossRef]
60. Lacina, K.; Skládal, P.; James, T.D. Boronic acids for sensing and other applications—A mini-review of papers published in 2013. *Chem. Cent. J.* **2014**, *8*, 60. [CrossRef]
61. Marques, M.E.; Mansur, A.A.P.; Mansur, H.S. Chemical functionalization of surfaces for building three-dimensional engineered biosensors. *Appl. Surf. Sci.* **2013**, *275*, 347–360. [CrossRef]
62. Li, M.; Xu, S.Y.; Gross, A.J.; Hammond, J.L.; Estrela, P.; Weber, J.; Lacina, K.; James, T.D.; Marken, F. Ferrocene-boronic acid-fructose binding based on dual-plate generator-collector voltammetry and square-wave voltammetry. *ChemElectroChem* **2015**, *2*, 867–871. [CrossRef] [PubMed]
63. Liu, S.; Shi, F.; Zhao, X.; Chen, L.; Su, X. 3-Aminophenyl boronic acid-functionalized $CuInS_2$ quantum dots as a near-infrared fluorescence probe for the determination of dopamine. *Biosens. Bioelectron.* **2013**, *47*, 379–384. [CrossRef]
64. Basiruddin, S.K.; Swain, S.K. Phenylboronic acid functionalized reduced graphene oxide-based fluorescence nano sensor for glucose sensing. *Mater. Sci. Eng. C* **2016**, *58*, 103–109. [CrossRef]
65. Li, D.; Zhang, Y.; Sun, F.; Felidj, N.; Gagey-Eilstein, N.; Lamouri, A.; Hémadi, M.; Nizard, P.; Luo, Y.; Mangeney, C. Dual-Probe SERS Nanosensor: A Promising Approach for Sensitive and Ratiometric Detection of Glucose in Clinical Settings. *ACS Appl. Bio Mater.* **2024**, *7*, 2254–2263. [CrossRef]
66. Orhan, E.; Garci, A.; Therrien, B. Flexible arene ruthenium metalla-prisms. *Inorg. Chim. Acta* **2015**, *438*, 5–9. [CrossRef]
67. Garci, A.; Dobrov, A.A.; Riedel, T.; Orhan, E.; Dyson, P.G.; Arion, V.B.; Therrien, B. Strategy to Optimize the Biological Activity of Arene Ruthenium Metalla-Assemblies. *Organometallics* **2014**, *3*, 3813–3822. [CrossRef]
68. Swamy, K.M.K.; Lee, Y.J.; Lee, H.N.; Chun, J.; Kim, Y.; Kim, S.-J.; Yoon, J. A New Fluorescein Derivative Bearing a Boronic Acid Group as a Fluorescent Chemosensor for Fluoride Ion. *J. Org. Chem.* **2006**, *71*, 8626–8628. [CrossRef]
69. Yan, J.; Springsteen, G.; Deeter, S.; Wang, B. The relationship among pKa, pH, and binding constants in the interactions between boronic acids and diols-it is not as simple as it appears. *Tetrahedron* **2004**, *60*, 11205–11209. [CrossRef]
70. Bull, S.D.; Davidson, M.G.; van den Elsen, J.M.H.; Fossey, J.S.; Jenkins, A.T.A.; Jiang, Y.-B.; Kubo, Y.; Marken, F.; Sakurai, K.; Zhao, J.; et al. Exploiting the Reversible Covalent Bonding of Boronic Acids: Recognition, Sensing, and Assembly. *Acc. Chem. Res.* **2013**, *46*, 312–326. [CrossRef]
71. Ortega-Valdovinos, L.R.; Valdes-García, J.; Bazany-Rodríguez, I.J.; Lugo-González, J.C.; Dorazco-González, A.; Yatsimirsky, A.K. Anion recognition by anthracene appended ortho-aminomethylphenylboronic acid: A new PET-based sensing mechanism. *New J. Chem.* **2021**, *45*, 15618–15628. [CrossRef]
72. Wu, X.; Chen, X.-X.; Jiang, Y.-B. Recent advances in boronic acid-based optical chemosensors. *Analyst* **2017**, *142*, 1403–1414. [CrossRef] [PubMed]
73. Cao, Z.; Cao, Y.; Kubota, R.; Sasaki, Y.; Asano, K.; Lyu, X.; Zhang, Z.; Zhou, Q.; Zhao, X.; Xu, X.; et al. Fluorescence Anion Chemosensor Array Based on Pyrenylboronic Acid. *Front. Chem.* **2020**, *8*, 414. [CrossRef]
74. Hargrove, A.E.; Nieto, S.; Zhang, T.; Sessler, J.L.; Anslyn, E.V. Artificial Receptors for the Recognition of Phosphorylated Molecules. *Chem. Rev.* **2011**, *111*, 6603–6782. [CrossRef]
75. Barry, N.P.E.; Furrer, J.; Freudenreich, J.; Süss-Fink, G.; Therrien, B. Designing the host-guest properties of tetranuclear arene ruthenium metalla-rectangles to accommodate a pyrene molecule. *Eur. J. Inorg. Chem.* **2010**, *2010*, 725–728. [CrossRef]
76. OpenAI. ChatGPT.4o (GPT-4). 2024. Available online: https://chat.openai.com (accessed on 25 June 2024).
77. Sasaki, Y.; Kubota, R.; Minami, T. Molecular self-assembled chemosensors and their arrays. *Coord. Chem. Rev.* **2021**, *429*, 213607. [CrossRef]
78. Lovrić, M.; Đuričić, T.; Tran, H.T.N.; Hussain, H.; Lacić, E.; Rasmussen, M.A.; Kern, R. Should we embed in chemistry? A comparison of unsupervised transfer learning with PCA, UMAP, and VAE on molecular fingerprints. *Pharmaceuticals* **2021**, *14*, 758. [CrossRef]
79. Sheini, A.; Khajehsharifi, H.; Shahbazy, M.; Kompany-Zareh, M. A chemosensor array for the colorimetric identification of some carboxylic acids in human urine samples. *Sens. Actuators B Chem.* **2017**, *242*, 288–298. [CrossRef]
80. Pham, D.T.; Dimov, S.S.; Nguyen, C.D. Selection of K in K-means clustering. *J. Mech. Eng. Sci.* **2005**, *219*, 103–119. [CrossRef]

81. Thordarson, P. Determining association constants from titration experiments in supramolecular chemistry. *Chem. Soc. Rev.* **2011**, *40*, 1305–1323. [CrossRef]
82. Bennett, M.A.; Smith, A.K. Arene ruthenium(II) complexes formed by dehydrogenation of cyclohexadienes with ruthenium(III) trichloride. *J. Chem. Soc. Dalton Trans.* **1974**, 233–241. [CrossRef]